Article:
Grimes, C. orcid.org/0000-0001-8261-218X, Button, C.A. orcid.org/0009-0005-2070-9548, Zhao, A. et al. (6 more authors) (2025) Cold sintering of α-alumina using functionalized boehmite: A cost-effective approach to reduce sintering temperature. Journal of the American Ceramic Society. e70208. ISSN: 0002-7820

https://doi.org/10.1111/jace.70208

Low temperature densification of α-alumina using cold sintered functionalised boehmite/α alumina composites: a cost-effective approach to reduce sintering temperature.

Christopher Grimes[1], Chloe A Button[1], Ao Zhao[1], Latham Haigh[1], Beatriz Almeida[1,2], Ines Vilarinho[2], M. Elisabete V. Costa[2], Eduardo Mantheakis[1] and Ian M Reaney[1].

[1]Functional Materials and Devices Laboratory
School of Chemical, Materials and Biological Engineering
University of Sheffield
Sheffield, S1 3JD

[2]Department of Materials and Ceramic Engineering/CICECO—Aveiro Institute of Materials,
Campus Universitário de Santiago,
University of Aveiro,
3810-193 Aveiro, Portugal.

Abstract

A novel cold assisted sintering process using a combination of functionalised boehmite and α–alumina particles is demonstrated. Functionalised boehmite and α-alumina composites were initially densified using a cold sintering process at <300 °C followed by heat-treatment at 1400-1450 °C (~200-300 °C lower than conventionally sintered α-alumina). Highest relative densities (98%) were achieved using meso-scale α-alumina (d_{50}=720 nm) in a 50:50 wt% mixture with boehmite, functionalised in 2M acetic acid. The high densities at low temperature were attributed to easy

propagation of the transformation to α phase within the dense boehmite matrix, accompanied by enhanced nucleation on the surface of the alumina particles. Critical aspects of the transformation sequence from functionalised boehmite to alpha alumina were characterised using Raman and Fourier Transform InfraRed spectroscopy. Preliminary hardness measurement were comparable with conventional alumina sintered at ~1650 °C and initial microwave measurements showed promise for the fabrication of high temperature co-fired ceramic substrates in electronics.

1 Introduction

Alumina, although a simple oxide, exhibits a complex crystal chemistry and undergoes a range of phase transition in which different polymorphs are thermodynamically stable at different temperatures, Figure 1.

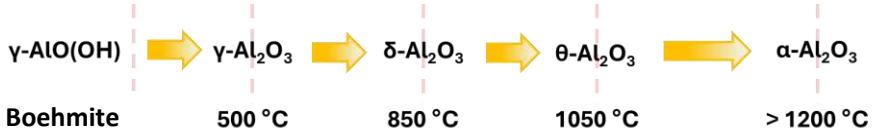

Figure 1: Polymorphic phase transitions of alumina based on heating hydrated raw materials such as gibbsite ($Al(OH)_3$) and boehmite.[1]

α-alumina is the most widely used of the alumina polymorphs in applications such as high temperature cofired ceramic substrates in electronics [2], hip joints [3, 4] and as refractories in the steel, glass and ceramic industries (bauxite bricks) [5, 6]. The only other polymorph of alumina that has been commercially exploited is γ-alumina [7, 8] which, in a lightly sintered form, is used as a porous catalyst support in the chemical industry [9, 10]. Both polymorphs may be formed from heat treatment at 400-500°C of the hydrated alumina minerals, boehmite (AlO(OH)) and gibbsite ($Al(OH)_3$). [1] However, even when pressed into a pellet, boehmite cannot be simply heat treated to give dense α-alumina due to differences in density and molar volume associated with the sequence of phase transitions shown in Figure 1, which can lead to microcracking and porosity.

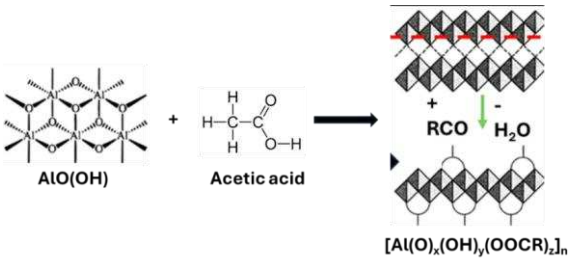

Figure 2: Crystal structure of boehmite and its functionalisation to form acetate alumoxane. [1, 11, 12]

Boehmite is a tetragonally distorted defect spinel with a cubic close packed anion lattice structure. The hydroxyl groups on the surfaces of each layer join to other hydroxyl groups in a zigzag arrangement of hydrogen bonds, parallel with the α-axis [1, 11, 12]. This arrangement facilitates functionalisation of the boehmite surface in accordance with the schematic shown in Figure 2. When boehmite reacts with a carboxylic acid (such as acetic acid, propionic acid or oxalic acid), cleaving occurs and carboxylate groups bind to the (100) plane (Figure 2), forming a carboxylate alumoxane, in this case acetate alumoxane (AlOOAc). The surface of boehmite particle therefore becomes functionalised and exhibits an enhanced solubility in water with respect to boehmite or alumina polymorphs. Carboxylate alumoxanes produced in this manner were investigated in the 1990s as a binder to lower the sintering temperature of α-Al_2O_3 [1, 11]**.**

The CSP is an ultra-low temperature (<300^{o}C) densification method based on hydrothermal sintering, known to geologists since the 1860's. [13] It has been shown to significantly reduce the sintering temperatures of many materials, such as: barium titanate, zinc oxide, alumina and magnetite [14-17]**.** In CSP, a small amount of transient solvent (a few wt.%) is mixed with the material to be sintered which is then placed in a die and pressed at moderate temperature and pressure, leading to densification. For greater details of the CSP, the reader is referred to refs 14-17. The mechanism(s) is/are however, still poorly understood and thought to involve pressure-solution creep prevalent in nature [17-19].

Cold sintering of α-alumina has been previously attempted by several research groups, but is challenging due to its chemical resistance, relying on either a high molarity acid [20], concentrated or solid strong base to act as a transient solvent [21], creating a composite of alumina with a material that actively cold sinters [22] or using cold sintering as part of a larger processing method (sometimes referred to as 'cold assisted sintering' [23, 24] to help lower the final sintering temperature [25]. Most notably Randall and co-workers, used cold assisted sintering to successfully achieved densification (97%) at 1400 ^{o}C, using glacial acetic acid (17.4M) as a transient solvent [20]. However, glacial acetic acid is highly corrosive and scaling up presents significant challenges in terms of safety, equipment compatibility, and process sustainability.

In this study, we present a benign, cost-effective method to densify α-alumina in which a 2M acetic acid (vinegar is ~0.9M) is used to functionalise pseudo-boehmite to form a surface coating of acetate alumoxane. The functionalised boehmite powder is then mixed with different volume fractions of α-alumina powder, cold sintered at up to 300^{o}C and then heat treated at 1400 ^{o}C/1450^{o}C to densify the

final pellet. The resulting densities and microstructures are investigated, along with preliminary hardness and microwave property measurements.

2 Experimental Procedure

2.1 Sample preparation

Pseudo-boehmite powder (Sasol ltd, >99.7% pure, <40nm) was ball-milled in isopropanol for 24 hours to break up agglomerates and then dried. For boehmite/α-alumina mixtures (100:0, 70:30, 50:50 and 30:70 wt%), the dried powders were weighed and combined with 2.0M acetic acid (25 ml/20 g) forming a slurry and wet milled for 10 hrs at 300 rpm. The slurry was then dried and the powder sieved and maintained at 80 ^{o}C for a further 48 hrs. For cold sintering, a few drops (~0.05 ml/g) of distilled water were added to the dried powder which was then mixed in a pestle and mortar and placed in a die and uniaxially pressed at up to ~350 MPa for 10 minutes at room temperature. The temperature was then raised to 125°C-300°C and held for 30-60 minutes (ramp rate 3.5-10 °C/min), followed by unassisted cooling to room temperature. Cold sintered and for comparison, conventionally pressed boehmite pellets were heated to 1400-1450^{o}C for 2 hours with a heating and cooling rate of 5 ^{o}C/min. In addition, batches were also made using α-alumina powder with course particles supplied by Pura (Lot:C11U024, CAS:1344-28, D_{50}= 2.6 μm) and finer particles provided Alpha Aesar (D_{50} 720 nm).

2.2 Density Measurements:

Geometrical Method: The diameter and thickness of the sample before and after heat treatment were measured using Vernier calipers with the average taken of multiple measurements. The mass was determined before and after heat treatment using a high-precision electronic balance with the average taken average from multiple measurements. The density of the sample was calculated before and after heat treatment using the following formula.

$$Density = \frac{Mass\ (g)}{Volume(cm^3)}$$

Archimedes Method: isopropanol (IPA) was used as the liquid medium thereby reducing errors caused by air entrapment. Isopropanol has a small molecular structure and can penetrate the porous structure of the sample. By thoroughly immersing the sample in isopropanol and using a Metter Toledo MS104S Newclassic MS analytical balance to measure the mass of the sample in air and water, the density of the sample was calculated from the following formula:

$$\rho_{measured} = \frac{Mass_{air}}{Mass_{air} - Mass_{liquid}}\left(\rho_{liquid} - \rho_{air}\right) + \rho_{air}$$

where $Mass_{air}$ is the mass of the sample in air, $Mass_{liquid}$ is the mass of the sample in isopropanol, ρ_{liquid} is the density of isopropanol, approximately 0.785g/cm3, and ρ_{air} is the density of air and approximately 1.225×10^{-3} g/cm^3. The theoretical densities of α–alumina and boehmite were 3.998 g/cm^3 and 3.049 g/cm^3, respectively. The theoretical density after mixing was calculated according using the following formula:

$$\rho_{theo,mix} = \frac{Mass_A \cdot \rho_A + Mass_B \cdot \rho_B}{Mass_A + Mass_B}$$

Relative density refers to the ratio of the actual measured density of a material to its theoretical density and was calculated using the following formula:

$$Relative\ density = \frac{\rho_{measured}}{\rho_{theoretical}}$$

2.3 Characterisation

Crystal phase analysis was performed with X-ray diffraction using Cu K_α radiation (Bruker, D2 PHASER and Malvern Aeris) at a step rate 0.02 °2θ. Raman spectra were collected using a Renishaw InVia Raman Microscope with 2400-g/mm grating with a 514.5 nm argon ion laser operating at 2 MW and 50x magnification. Spectra were collected for 15 s and 10 accumulations. Spectra were background-subtracted using an asymmetric least squares approach and smoothed using a Savitsky-Golay filter with a data window of 5 points and a 2nd order polynomial fit. For FTIR, sodium bromide was ground with the sample (99:1) in a mortar and pestle before cold pressing. A blank of sodium bromide was used for the background scan which was automatically removed from the spectra. Scanning electron microscopy (SEM) was carried out on a FEI, Inspect F50, with analysis of the microstructure performed using ImageJ software.

Hardness tests were undertaken on a Mitutoyo I9 Indenter with 10 individual Vickers hardness measurements taken from the top and cross section of the densest pellets produced using both sizes of α-Al_2O_3. Microwave dielectric properties were measured using the TE_{011} mode with a network analyser (ADVAMTEST R3767CH) and a Cu cavity.

3 Results and Discussion

3.1 Fabrication of α-alumina

3.1.1 Pellets produced using coarse α-alumina (D_{50}=2.6µm)

Three functionalised boehmite/α-Al_2O_3 composites were produced, all of which were successfully cold sintered and annealed at 1400°C to produce pellets which exhibited a single phase in XRD patterns (α-Al_2O_3 ICDD ref. 04-005-4213, Figure 3), confirming complete transformation of boehmite into α-Al_2O_3.

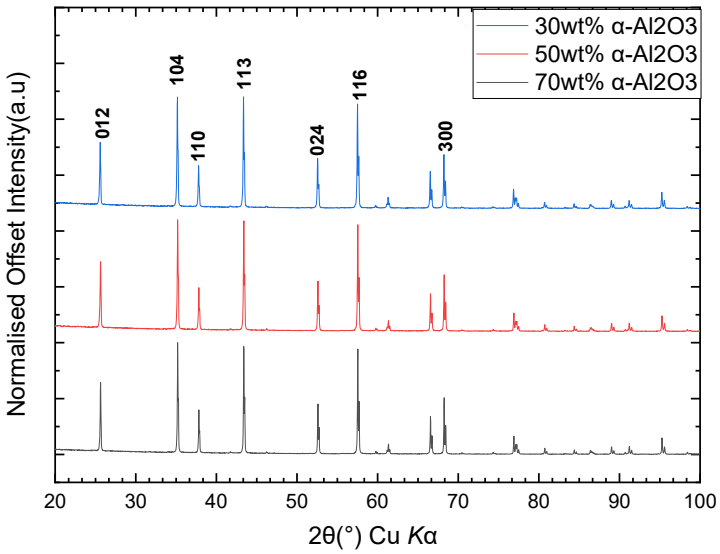

Figure 3: Comparison of the XRD pattern obtained from the annealed ceramic pellets produced from boehmite/α-Al_2O_3 compositions containing 70% (blue), 50% (red) and 30% (black) α-Al_2O_3.

XRD, Raman and FTIR were also conducted at key points during the process to monitor changes in the crystal form, amorphous content and understand transformational pathway, the results from which are presented and discussed in section 3.3. The final density of the pellets increased with increasing boehmite concentration with an average relative density of 95% achieved for the 30% α-Al_2O_3 -70% boehmite after heat treatment at 1400 °C, **.**

Table 1 **. The microstructure of pellets with the highest density was analysed using imageJ software which gave an average grain size of 0.95µm with a standard deviation 0.48. (Figure 4). The difference in average grain size to the starting a alumina particle size is attributed to the presence smaller grains/particles which arise from the decomposition of boehmite.**

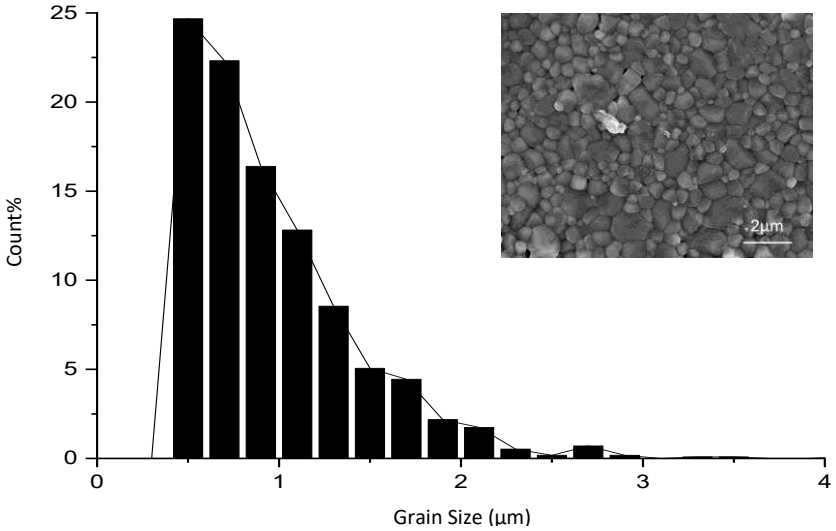

Figure 4: Grain size analysis of the α-Al_2O_3 ceramic pellets (30:70 alpha:boehmite) sintered at 1400 °C using micron size α-Al_2O_3. Inset is the SEM image used to obtain the analysis.

Table 1: Relative density for various pellet ratios using 2M acetic acid and heat treated at 1400 °C.

Ratio		Final Relative density (%)	**CSP Relative density (%)**
α–alumina	boehmite		
100	0	53±2.0	**51±3**
70	30	56±2.0	**54±2**
50	50	83±1.0	**64±2**
30	70	95±2.0	**73±1**

The densification achieved for 30:70 alumina:boehmite pellets is similar to that for conventional sintering using pure alumina powder at 1650°C [25], suggesting that scaling of the process could potentially lead to energy savings in the production of undoped Al_2O_3 components [15].

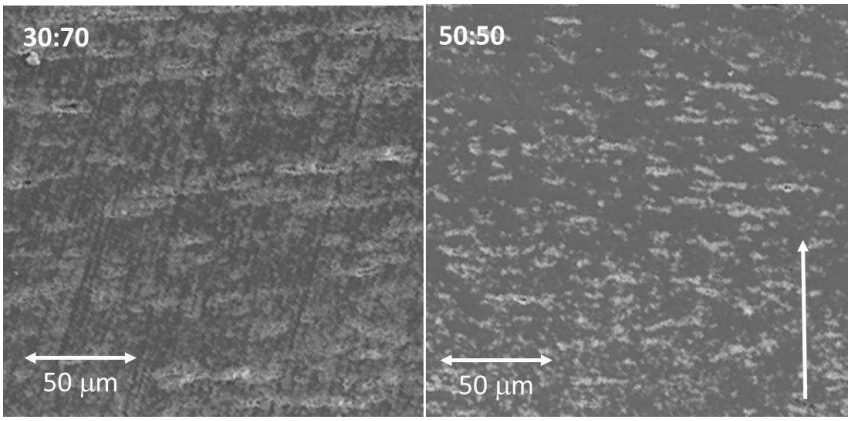

Figure 5: SEM micrographs of 30:70 and 50:50 α-Al_2O_3/boehmite pellets with the pressing direction indicated.

However, SEM images of polished cross sections revealed penny shaped flaws normal to the pressing direction for 50:50 and 30:70 samples, Figure 5. The exact cause of these defects remains unknown but they may relate to the large size difference between the functionalised pseudo boehmite and α-Al_2O_3 particles which leads to internal stress during densification or they could result from trapped CO_2/water vapour from the decomposition of the acetate alumoxane resulting in voids too large to be removed via sintering.

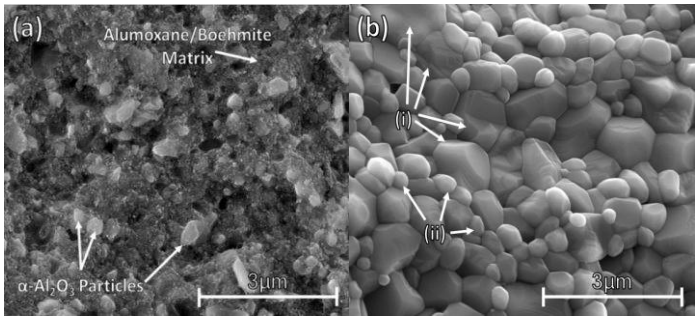

Figure 6: Scanning electron micrographs of fracture surfaces of 50:50 samples a) cold sintered and b) cold sintered followed by heat treatment at 1400 °C.

Figure 6 shows the fracture surfaces of a 50:50 ceramic after a) the cold sinter step and b) densification at 1400 °C. In Figure 6a, α-alumina particles are suspended within a matrix of boehmite/acetate alumoxane which does not exhibit a clearly defined grain structure. After heat treatment at 1400°C, the formation of α-Al_2O_3 is complete and the grain structure shows classic triple junctions and equiaxed grains (Figure 6b). Fracture of the pellets occurred dominantly along

the weakest points in the microstructure, i.e. the flaws normal to the pressing direction, and therefore represents the densification/grain morphology at the surface of the void. Nonetheless, it clearly shows the potential of this method to create dense alumina bodies at ~250 °C lower than for conventionally sintered parts. Xie et al noted that the introduction of alumina particles not only lowered the transformation to the α phase to ~ 1100°C in boehmite but also enhanced the rate in which the transformation occurred. [26] The size of these grains appeared to be similar to that of the alumina powder particles used as the input material (1-2μm), consistent with Messing et al who stated that incorporation of α-alumina particles in boehmite offered formidable control over the grain size [27].

3.1.2 Pellets formed using meso powder of α alumina (D_{50}=720 nm)

The penny shaped flaws described in section 3.1.1 constitute unacceptable defects in an alumina body and would lead to low bend strength and fracture toughness. Hence, it is imperative that they are eliminated if the cold assisted sintering of α–alumina is to be commercially viable. As described previously, the most likely explanations for the appearance of the flaws are poor distribution/mixing of the large α-alumina particles or trapped gases that leave voids that are too large to be eliminated through a conventional sintering step at 1400 °C. **In addition, during processing of samples with micron sized alumina particles, higher densities were more reproducibly achieved at 1450 °C rather than 1400 °C.** It is logical therefore to not only increase the sintering temperature but to also reduce the particle size of α-alumina in the cold sintered body.

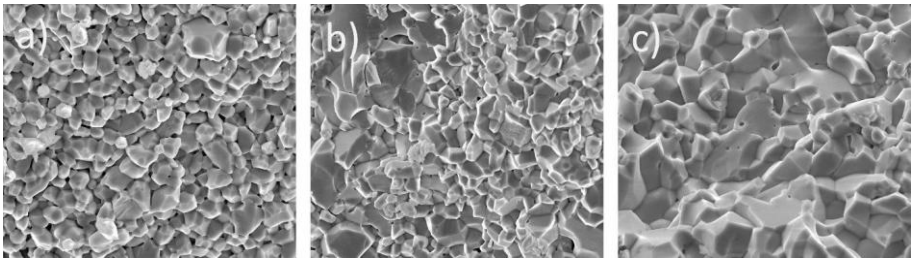

Figure 7: SEM images of fracture surfaces of 30:70 sample, heat treated at 1450 °C but cold sintered at) 125 °C, b) 150 °C, and c) 200 °C.

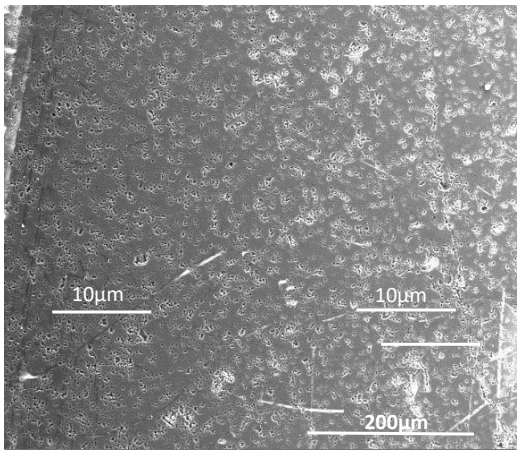

Figure 8: SEM micrograph of cross-section for ceramic produced from meso α-Al_2O_3 (50:50,125°C,250MPa).

Meso α-Al_2O_3 particles (D_{50} 720nm) were therefore used and the work replicated at 1450 °C. Figure 6 shows SEM images of fracture surface from samples cold sintered at 125 °C, 200 °C and 300 °C and then annealed at 1450 °C. Cold sintering temperature had little effect on final density with all conditions producing a post-heat treatment density >95%, far greater than α–alumina conventionally sintered at 1450 °C and competitive with samples sintered at 1650 °C. Samples cold sintered at 125°C showed more irregular shaped grains with porosity and microcracks throughout but increasing the cold sintering step resulted in a more homogeneous microstructure with larger regular grains and fewer pores, consistent with a relative density approaching 100 % (Figure 7). Most importantly the penny shaped defects were no longer present when cross-sections were analysed by SEM (Figure 8). Image analyses of the SEM cross-sections are largely in agreement with the geometric densities. **Grain size analysis was conducted on the densest ceramic pellet using meso-powder (figure 9). The grain size was similar to the starting particle size of the alumina (720nm) with a standard deviation of 0.36.**

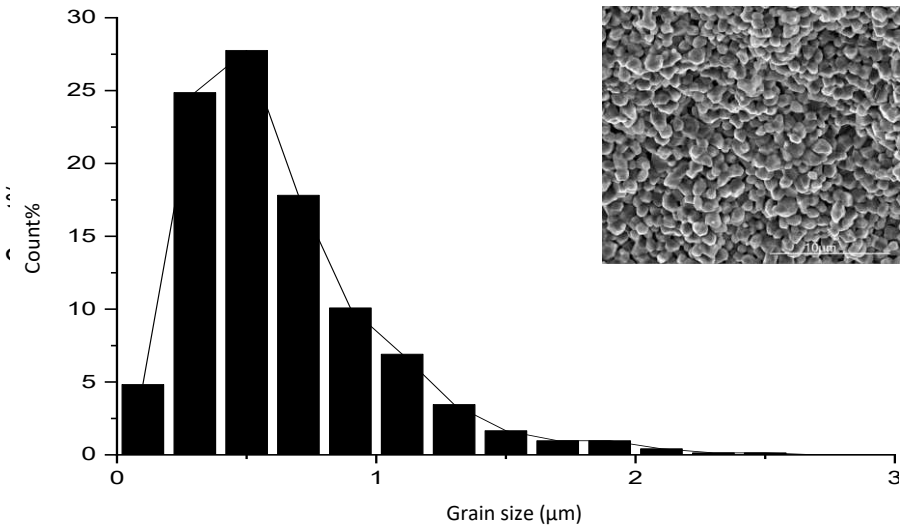

Figure 9: Grain size analysis of the final α-Al_2O_3 ceramic pellets (50:50 alpha:boehmite) using meso size α-Al_2O_3 particles cold sintered at 125°C then sintered at 1450 °C. Inset is an SEM image of the region of the sample used for analysis

Table 2: Ceramic ratio, cold sinter temperature and density after heat treatment at 1450°C for pellets fabricated using meso α-alumina powder.

Composite ratio		Cold sintering Temperature(°C)	Final Relative density (%)	**CSP only relative density (%)**
α-Al_2O_3	boehmite			
100	0	NA	78	**59**
70	30	125	95	**72**
		150	93	**72**
		200	98	**73**
50	50	125	98	**66**
30	70	125	96	**65**

3.2 Characterisation of α–alumina

3.2.1. Hardness measurements

Within the limited data set, cold assisted sintered samples exhibited equivalent (1930 kg/mm^2) or superior hardness to their conventionally sintered counterparts (1800 kg/mm^2). Whilst comprehensive mechanical property measurements are still required, the hardness tests and high density of the cold assisted sintered α-alumina show great promise for commercial applications.

Table 3: Comparison of conventionally sintered commercially available alumina ceramics with alumina ceramics produced using the optimal cold sintering process conditions for their respective particle sizes.

Ceramic	Average Vickers hardness (Kg/mm^2)	
	Surface	Cross section
30% Micron Alumina 70% Boehmite	>1930	>1930
50% Meso Alumina 50% boehmite	1852	1809
Aloxalon 999 by International Syalons (29)	1800	
Accuratus Ceramic Corporation. 99.5% Alumina (30)	1440	

3.2.2 Microwave dielectric measurements

Preliminary measurements of microwave (MW) quality factor (Q*f*) and permittivity (ε_r) were also obtained for the cold assisted sintered samples made using meso-sized α-alumina, Figure 10. Q*f* was maximum (3700 GHz) for samples cold sintered at 125 °C but decreased with cold sintering temperature. Increasing the percentage of boehmite decreased both ε_r and Q*f* from 4400, 9.98 (0 %) to 2400, 9.68 (100%). These preliminary results demonstrate that the α–alumina ceramics exhibit a MW dielectric response but further work is required to optimise their properties. **It is likely however, that the higher the boehmite concentration, the smaller the average grain size which is known to decrease Q*f* due to the high grain boundary area. (ref) The transition to a alumina may also increase the number of point defects and dislocation in the structure, both of which would negatively affect Q*f*. (ref)**

Commented [ir1]: Microwave dielectric ceramics for resonators and filters in mobile phone networks, Ian M Reaney, David Iddles, J. Am. Ceram. Soc. 89(7), 2063-2072 (2006)

Commented [ir2]: As above

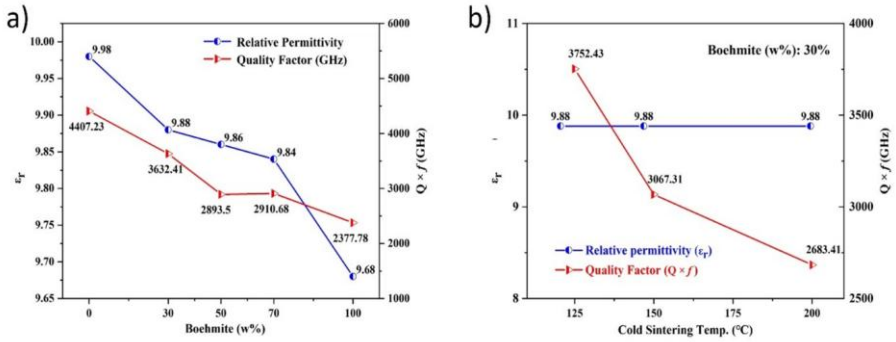

Figure 10: Microwave dielectric properties (permittivity, ε_r and quality factor, Qf) as a) function boehmite concentration (125 °C/250MPa) and b) cold sintering temperature (250 MPa). All samples had a final sinter at 1450 °C.

1.3 Boehmite to α-alumina transformation

The transformation of the initial functionalised 50:50 boehmite-alumina mixture to the final pure alumina ceramic was monitored using XRD (Figure 11), Raman (Figure 12) and FTIR (Figure 13). As expected, samples heat-treated at 1450 °C showed complete conversion to pure α-Al_2O_3 in accordance with literature [1]. XRD showed changes in peak intensities and positions for both cold sintered and heat-treated samples, compared with the starting functionalised boehmite/α-alumina powder. Cold sintered material (pre-heat treatment) shows broadening of the boehmite XRD peaks along with the disappearance of the major peak at 15 °2θ. **Broadening and disappearance of peaks have previously been observed for boehmite [28, 29] as a result of decomposition which in our case leads to a reduction in the effective diffracting volume without the material becoming fully amorphous**. Acetate alumoxane was not observed in any XRD data, likely due to a combination of a low volume fraction and/or because of its amorphous nature.

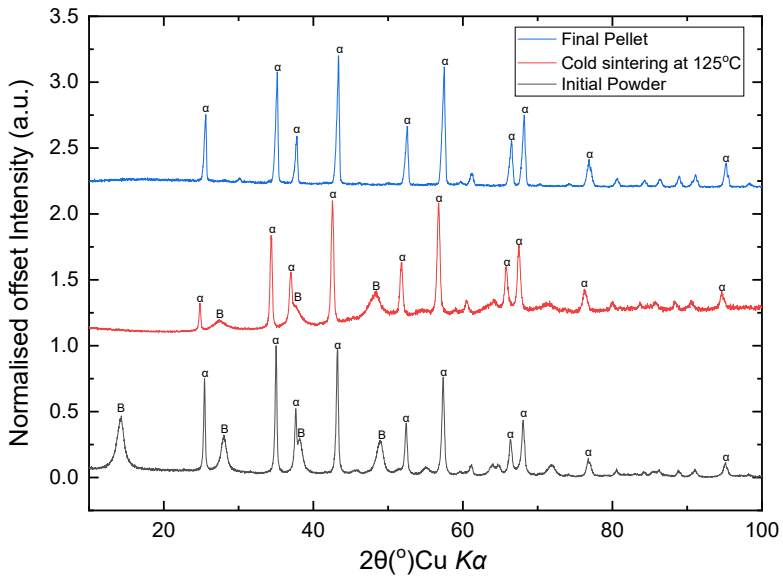

Figure 11: XRD patterns from the initial powder (black), after CSP (250 MPa, 125°C, red) and after heat treatment (250 MPa, 125°C , 1450°C, blue) using 50:50 wt.% boehmite/meso α-Al_2O_3 composite.

Consistent with XRD, Raman spectroscopy (Figure 10) revealed several low frequency modes for boehmite such as at 377 and 497 cm^{-1} and for α-Al_2O_3, most notably at 417 cm^{-1}. A third phase with a distinct set of modes which could not be attributed to boehmite or α-alumina but consistent with acetate salts was also observed [30-32] and interpreted here as arising from acetate alumoxane on the surface of boehmite, e.g. 1427 cm^{-1} (Figure 10, Table 4).

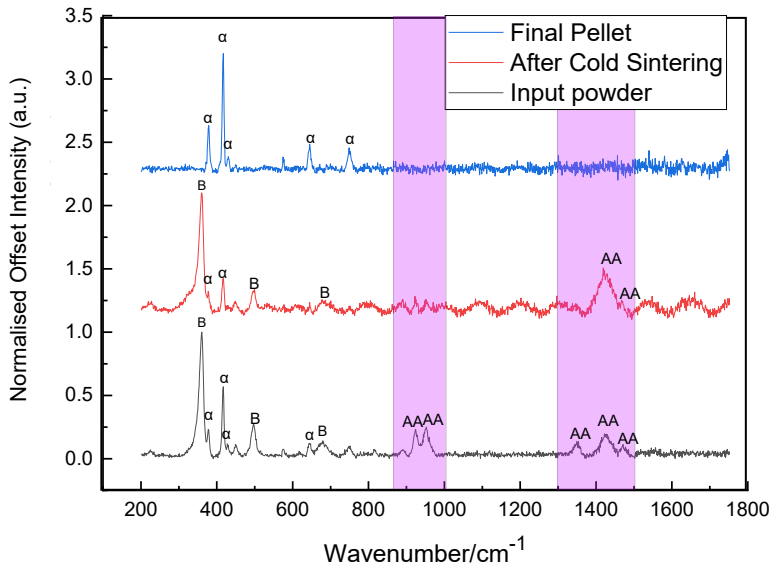

Figure 12: Raman spectrum from the initial 50:50 wt% boehmite/ meso α-Al_2O_3 composite (black), after the CSP (250MPa, 125°C, red) and after heat treatment process (250MPa, 125°C, 1450 °C, blue). Modes associated with the presence of acetate alumoxane (AA), alpha alumina (α) and boehmite (B) [30-32] are assigned.

After cold sintering at 125°C/250 MPa, the acetate alumoxane, boehmite and α–alumina peaks were retained. Consistent with XRD, Raman analysis confirmed that after annealing at 1450 °C the only modes present were associated with α-alumina.

Table 4: Raman mode allocations for α-alumina, boehmite and acetate alumoxane.

Compound	Symmetry Class	Wavenumber (cm^{-1})		
		Input powder	After cold sintering	Final Pellet
α-Al_2O_3	A_{1g}	417, 643, 687		417,644
	A_{2g}	749		
	A_{2u}		495	
	E_{u1}		377	
	E_g	377, 430, 574		378, 430, 447, 576, 748
Boehmite	A_g	360, 497, 679	360	
	B_{2g}	445	343, 450	
Acetate Alumoxane	A_{1v1}	1427	1421	
	A_{1v2}	1354		
	A_{1v3}	677		
	A_{1v4}	920	922	
	B_{1v9}	1451		

Concomitant with Raman, FTIR spectroscopy of the initial powder showed the presence of acetate groups at ~1560 cm^{-1} along with O-H associated with boehmite at 3200 cm^{-1} (Figure ,Table 5). As cold sintering temperature increased, the relative intensities of peaks associated with the acetate group decreased whilst the O-H bond peak increased in intensity.

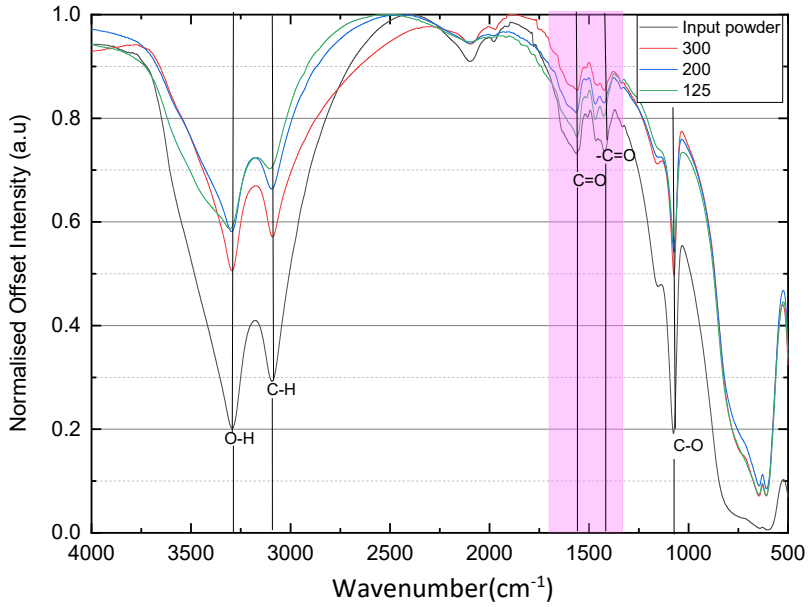

Figure 13: FTIR spectra of 50:50 functionalised Boehmite/α-Al_2O_3 powder(black) after being cold sintered at 250MPa at 125°C (green), 200°C (blue) and 300°C (red).

Table 5: Mode allocations for the FTIR spectra of 50:50 wt% functionalised boehmite/α-Al_2O_3 provided by ref. *[33]* .

Compound	Bond	Wavenumber (cm^{-1})			
		Input powder	125°C	200°C	300°C
Boehmite	**O-H**	3320	3319	3316	3321
Acetate alumoxane	**C=O**	1564	1559	1621	1563
	C-O	1075	1071	1073	1073
	C-C=O	1420	1424	1422	1424
	C-H	3095	3090	3097	3088

It is hypothesised that as pressure and heat are applied to the acetate alumoxane/boehmite/α-Al_2O_3 composites, functionalised boehmite along with the boehmite partially decompose during the cold sintering step, accelerated by increasing temperature. However, complete decomposition of the acetate alumoxane and boehmite does not occur under the conditions used within this study. At higher cold sintering temperatures (300 °C), it also remains unknown whether amorphous alumina is

present since this is reported as a product of the decomposition of acetate alumoxane [34]. At 1450°C, composites are completely transformed into α-Al_2O_3. Future studies would benefit from more extensive in-situ XRD/FTIR/Raman studies of the transformation process.

The use of functionalised boehmite to form acetate alumoxane in a cold sintered process is key to increasing the final density and decreasing the sintering temperature of α-alumina. α-Al_2O_3 powder within the initial composition seeds the transformation to the high temperature polymorph and enhances the rate of phase transformation. Previous work has discussed the use of alumoxanes as a binder material to improve alumina sintering [35] as part of a slip-casting process, however, to date its use in a CSP has not been reported. A pressure-solution creep rearrangement process is most likely to take place due to the solubility of the acetate alumoxane in water, similar to the ZnO/Zn-acetate system. In conventional sintering a higher starting "green" density > 40 % theoretical only contributes to the rate but has little effect on final densification [36, 37]. However, it is proposed that the nucleation process inherent in the growth of α-alumina from boehmite, [38-40] is responsible for the lower densification temperatures.

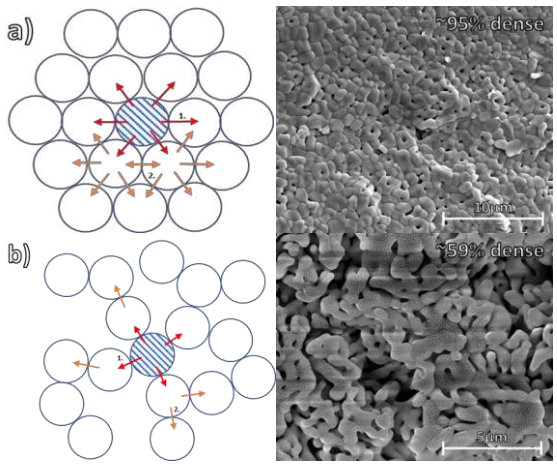

Figure 12: Schematic illustrating to role of α-Al_2O_3 seeding in densification: a) shows the better packing of alumina/boehmite matrix post cold sintering which leads to a denser pellet and more rapid transformation compared to b) in which a pure boehmite matrix transforms but more slowly due to a lower packing density and the absence of α-alumina seeds during cold sintering.

The microstructures therefore, observed in this study result from an α-alumina 'seeding' process similar to that described by refs [38-40] where 1-10 wt% of pre-transformed α-or-γ alumina powder was introduced into boehmite. The α-alumina particles act as epitaxial nucleation sites. Pach et al.

[40] found that without seeding, nuclei will appear in zones of dense hexagonal packing where the coordination number is at its highest. The closer packing of the cold sintered boehmite leads to larger concentration of these favourable nucleation points, as well as more rapid transformation and grain growth. Evidence for this is found from the network-like structure observed in samples, sintered conventionally from pressed boehmite, as well as the presence intra-granular pores, often linked to rapid grain growth [41]. A diagram illustrating this hypothesis is shown in Figure 12. This mechanism is entirely consistent with the increase in density associated with the use of meso- rather than micro-scale particles of α-alumina in the composite mixture with functionalised boehmite. The use of smaller particles increases the surface area of α-alumina seeds enhancing the rate and increasing the homogeneity of the phase transformation to the high temperature polymorph.

The decrease in sintering temperature with respect to conventional α–alumina in this study is ~200-250 ^{o}C. The total energy saving is therefore significant since radiative heat loss is proportional to T^4 according to the Stefan-Boltzman equation which means even small changes in sintering temperature can decrease the cost of production. In addition, for electric furnaces, a 200 ^{o}C, reduction in sintering temperature permits the use of more robust and cheaper SiC rather than MoS_2 based heating elements, thereby decreasing capital costs. Optimum densities (98 %) were achieved for meso- (d_{50} = 720 nm) rather than nanopowders along with functionalised boehmite. The cold assisted sintering process therefore avoids the use of expensive nano-powders. Functionalised boehmite is used commercially as a binder for slip cast alumina and is consequently also relatively inexpensive.

Kang et al achieved promising densities at 100°C lower than the current work following a cold sintering step. However, these authors used more expensive nano-alumina particles (100 nm) and their transient solvent was glacial (17.5M) as opposed to 2m acetic acid. Nano-alumina is already known to densify at 1350-1400 ^{o}C and therefore the approach does not strictly result in a significant decrease in sintering temperature when the particle size of the starting powder is taken into account. The use of glacial acetic acid would also result in significant health and safety issues if the process were to be scaled.

4 Conclusions

High density, undoped α-Al_2O_3 ceramics were fabricated using a novel process, comprising cold sintering of α-alumina/functionalised boehmite powder followed by heat treatment at 1400/1450 ^{o}C. Final ceramic pellets achieved densities and hardness similar to conventional ceramics sintered at significantly higher temperatures (1650 ^{o}C). Preliminary MW property measurements revealed ε_r ~

10 typical for α-alumina with optimum Q*f* values approximately, 3700 GHz when cold sintered at 125 °C. The use of micron sized particles repeatedly resulted in the formation of penny-shaped cracks normal to the pressing direction when sintered at 1400 °C. Sintering at higher temperature and the use of meso-sized α-alumina gave higher densities and eliminated the penny shaped flaws. A reduction of 200 °C in sintering temperature with respect to conventional α-alumina not only reduces energy usage but also facilitates a reduction in capital expenditure through the use cheaper more robust SiC with respect to MoS_2 heating elements.

5 Acknowledgements

The authors acknowledge Engineering Physical Science Research Council grants No EP/X016463/1, the InnovateUK 'Economiser' programme, CICECO-Aveiro Institute of Materials, Projects UIDB/50011/2020, UIDP/50011/2020 and LA/P/0006/2020 funded through the FCT/MCTES (PIDDAC) and the Journal of European Ceramic Society Trust (JECS Trust mobility grant Contract n2022308).

6 References

1. Callender, R.L., et al., *Aqueous Synthesis of Water-Soluble Alumoxanes: Environmentally Benign Precursors to Alumina and Aluminum-Based Ceramics.* Chemistry of Materials, 1997. **9**(11): p. 2418-2433.
2. Prasad, V.C.S., *Alumina Ceramics for the Electronic Industry—Part I.* Transactions of the Indian Ceramic Society, 1982. **41**(3): p. 51-63.
3. Cai, Y.Z. and S.G. Yan, *Development of ceramic-on-ceramic implants for total hip arthroplasty.* Orthop Surg, 2010. **2**(3): p. 175-81.
4. Ben-Nissan, B., A.H. Choi, and R. Cordingley, *10 - Alumina ceramics*, in *Bioceramics and their Clinical Applications*, T. Kokubo, Editor. 2008, Woodhead Publishing. p. 223-242.
5. Ruys, A.J.a., *Alumina Ceramics : Biomedical and Clinical Applications*. 2019.
6. Gürel, S.B. and A. Altun, *Reactive alumina production for the refractory industry.* Powder Technology, 2009. **196**(2): p. 115-121.
7. Keshavarz, A.R., M. Rezaei, and F. Yaripour, *Nanocrystalline gamma-alumina: A highly active catalyst for dimethyl ether synthesis.* Powder Technology, 2010. **199**(2): p. 176-179.
8. Schiffino, R.S. and R.P. Merrill, *A mechanistic study of the methanol dehydration reaction on .gamma.-alumina catalyst.* The Journal of Physical Chemistry, 1993. **97**(24): p. 6425-6435.
9. Krokidis, X., et al., *Theoretical Study of the Dehydration Process of Boehmite to γ-Alumina.* The Journal of Physical Chemistry B, 2001. **105**(22): p. 5121-5130.
10. Trueba, M. and S.P. Trasatti, *γ-Alumina as a Support for Catalysts: A Review of Fundamental Aspects.* European Journal of Inorganic Chemistry, 2005. **2005**(17): p. 3393-3403.
11. Landry, C.C., et al., *From minerals to materials: synthesis of alumoxanes from the reaction of boehmite with carboxylic acids.* Journal of Materials Chemistry, 1995. **5**(2): p. 331-341.

12. Tettenhorst, R. and D.A. Hofmann, *Crystal Chemistry of Boehmite.* Clays and Clay Minerals, 1980. **28**(5): p. 373-380.
13. Sorby, H.C., *The Bakerian Lecture: On the Direct Correlation of Mechanical and Chemical Forces.* Proceedings of the Royal Society of London, 1862. **12**: p. 538-550.
14. Grasso, S., et al., *A review of cold sintering processes.* Advances in Applied Ceramics, 2020. **119**(3): p. 115-143.
15. Guo, J., et al., *Cold Sintering: A Paradigm Shift for Processing and Integration of Ceramics.* Angewandte Chemie International Edition, 2016. **55**(38): p. 11457-11461.
16. Maria, J.-P., et al., *Cold sintering: Current status and prospects.* Journal of Materials Research, 2017. **32**(17): p. 3205-3218.
17. Ndayishimiye, A., et al., *Roadmap for densification in cold sintering: Chemical pathways.* Open Ceramics, 2020. **2**: p. 100019.
18. McCLAY, K.R., *Pressure solution and Coble creep in rocks and minerals: a review.* Journal of the Geological Society, 1977. **134**(1): p. 57-70.
19. Shimizu, I., *Kinetics of pressure solution creep in quartz: theoretical considerations.* Tectonophysics, 1995. **245**(3): p. 121-134.
20. Kang, S., et al., *Thermal-assisted cold sintering study of Al2O3 ceramics: Enabled with a soluble γ-Al2O3 intermediate phase.* Journal of the European Ceramic Society, 2023. **43**(2): p. 478-485.
21. Grady, Z., A. Ndayishimiye, and C. Randall, *A dramatic reduction in the sintering temperature of the refractory sodium β''-alumina solid electrolyte via cold sintering.* Journal of Materials Chemistry A, 2021. **9**(38): p. 22002-22014.
22. Induja, I.J. and M.T. Sebastian, *Microwave dielectric properties of cold sintered Al2O3-NaCl composite.* Materials Letters, 2018. **211**: p. 55-57.
23. Kholodkova, A.A., et al., *Water-Assisted Cold Sintering of Alumina Ceramics in SPS Conditions.* Ceramics, 2023. **6**(2): p. 1113-1128.
24. Liu, J., B. Liu, and K.X. Song, *Enhanced microwave dielectric properties of Al2O3 ceramics via a cold sintering assisted two-step sintering route.* Journal of Materials Science: Materials in Electronics, 2024. **35**(11): p. 764.
25. William H. Rhodes, G.C.W., George A. Fryburg., *Rapid-sintering of alumina*. 1987, Osram Sylvania Inc: United States.
26. Xie, Z.-P., et al., *Influence of different seeds on transformation of aluminum hydroxides and morphology of alumina grains by hot-pressing.* Materials & Design, 2003. **24**(3): p. 209-214.
27. Messing, G.L., *Seeding of Transformations*, in *Concise Encyclopedia of Advanced Ceramic Materials*, R.J. Brook, Editor. 1991, Pergamon: Oxford. p. 409-411.
28. Takagaki, A., J.C. Jung, and S. Hayashi, *Solid Lewis acidity of boehmite γ-AlO(OH) and its catalytic activity for transformation of sugars in water.* RSC Advances, 2014. **4**(82): p. 43785-43791.
29. Cabral, A.A., et al., *Effect of the milling conditions on the decomposition kinetics of gibbsite.* Boletín de la Sociedad Española de Cerámica y Vidrio, 2023. **62**(3): p. 292-301.
30. Frost, R.L. and J.T. Kloprogge, *Raman spectroscopy of the acetates of sodium, potassium and magnesium at liquid nitrogen temperature.* Journal of Molecular Structure, 2000. **526**(1): p. 131-141.
31. Kiss, A.B., G. Keresztury, and L. Farkas, *Raman and i.r. spectra and structure of boehmite (γ-AlOOH). Evidence for the recently discarded D172h space group.* Spectrochimica Acta Part A: Molecular Spectroscopy, 1980. **36**(7): p. 653-658.
32. Liu, Y., et al., *Study of Raman spectra for γ-Al2O3 models by using first-principles method.* Solid State Communications, 2014. **178**: p. 16-22.
33. Mecozzi, M. and E. Sturchio, *Computer Assisted Examination of Infrared and Near Infrared Spectra to Assess Structural and Molecular Changes in Biological Samples Exposed to Pollutants: A Case of Study.* Journal of Imaging (J. Imaging), 2017. **3**.

34. Boretskaya, A., et al., *Identification of amorphous and crystalline phases in alumina entity and their contribution to the properties of the palladium catalyst.* Applied Surface Science, 2019. **496**: p. 143635.
35. Loscutova, R. and A.R. Barron, *Application of alumoxane nanoparticles as precursors for 3D alumina features.* Journal of Materials Science, 2006. **41**(11): p. 3391-3401.
36. Rahaman, M.N., L.C. De Jonghe, and M.-Y. Chu, *Effect of Green Density on Densification and Creep During Sintering.* Journal of the American Ceramic Society, 1991. **74**(3): p. 514-519.
37. WOOLFREY, J.L., *Effect of Green Density on the Initial-Stage Sintering Kinetics of UO2s.* Journal of the American Ceramic Society, 1972. **55**(8): p. 383-389.
38. KUMAGAI, M. and G.L. MESSING, *Controlled Transformation and Sintering of a Boehmite Sol-Gel by α-Alumina Seeding.* Journal of the American Ceramic Society, 1985. **68**(9): p. 500-505.
39. Nordahl, C.S. and G.L. Messing, *Sintering of α-Al2O3-seeded nanocrystalline γ-Al2O3 powders.* Journal of the European Ceramic Society, 2002. **22**(4): p. 415-422.
40. Pach, L., R. Roy, and S. Komarneni, *Nucleation of alpha alumina in boehmite gel.* Journal of Materials Research, 1990. **5**(2): p. 278-285.
41. Rahaman, M.N., *Ceramic Processing and Sintering*. 2017.
42. Prins, R., *On the structure of γ-Al2O3.* Journal of Catalysis, 2020. **392**: p. 336-346.